Understanding the Degradation of MEA in PEMFC: Definition of Structural Markers and Comparison Between Laboratory and On-Site Ageing

Gilles De Moor,[1] Corine Bas,[1] Freddy Lesage,[1] Anne Sophie Danérol,[1] Eric Claude,[2] Elisabeth Rossinot,[2] Marion Paris,[2] Lionel Flandin,[1] Nicole Dominique Albérola[1]

[1]*Laboratoire Matériaux Organiques à Propriétés Spécifiques (LMOPS), UMR 5041, Université de Savoie, Campus Scientifique, 73376 Le Bourget-du-Lac Cedex, France*
[2]*Axane/AL-H2E, 2 rue de Clémencière BP-15, 38360 Sassenage, France*

Received 20 May 2010; accepted 2 October 2010
DOI 10.1002/app.33506
Published online 14 February 2011 in Wiley Online Library (wileyonlinelibrary.com).

ABSTRACT: Different accelerated tests in 12 fuel cells stack were performed in laboratory, namely on/off, back-up, and base-load regimes. In parallel, membrane electrode assemblies (MEA) were integrated in two "on-site" systems for GSM relay application. One of them was dedicated to base-load power applications while the second fuel cells coupled with photovoltaic panels operated in semibase load mode. To investigate the influence of the power profiles on MEA degradation, over 80 CCB MEAs (5 layers) were studied at different scales using *ex situ* characterizations such as tensile tests, TGA-MS, DMTA, and SEM. A series of complementary microstructural ageing markers were thereby identified. The isolated influence of dry-wet cycling on MEA properties was also established after passive hydro-thermal (HT) ageing performed continuously for 10 months in the laboratory. The changes of each marker as a function of HT ageing time permitted to define a temporal benchmark. Based on these indicators, the main changes occurred in the MEA properties appear after a 5 months dry-humid cycling (up to about 1800 cycles). The trends observed were useful to compare and estimate the degree of degradation of each ageing tests. Thus, the accelerated tests performed in laboratory for at least 500 h in stack did not reveal systematic MEA modifications. On the contrary, the 1500 h "on-site" system operation results in some MEA degradations which origins are discussed. © 2011 Wiley Periodicals, Inc. J Appl Polym Sci 120: 3501–3510, 2011

Key words: degradation; fluoroploymers; structure-property relations; mass spectrometry

INTRODUCTION

Proton exchange membrane fuel cell (PEMFC) system is one the most promising energy converters to produce efficient and environmentally friendly energy for various applications such as portable, automotive, or stationary applications. Improving the durability of membrane electrode assembly (MEA) is one of the most important challenges to overcome for a successful commercialization. The MEA also referred as "the heart of the fuel cell" is made of a membrane electrolyte coated with active layers (AL) at each side and covered by gas diffusion layers (GDL). Two main accelerated degradation tests are described in the literature. The most famous one is the Fenton test which is based on the chemical degradation mechanism. The Fenton test is conducted using H_2O_2 solution and few ppm metal ions in a 50–90°C temperature range.[1–4] Fenton test seems to strongly depend on H_2O_2 quality, especially the amount of cations, and the severe chemical degradation does not permit to properly estimate the membranes' behavior in the application.[5] The other accelerated ageing technique is the so-called open circuit voltage (OCV) which mainly degrades the active components of the MEA.[6,7] This technique also presents drawbacks, and hardly compares with real applications. Further works were thus performed to study the degradation mechanisms of each component. The membrane degradation is thought to originate from different mechanisms such as: chemical attack of end groups by hydroxyl or peroxy radicals[8,9]; mechanical failure induced by high differential in gas pressure or by puncture and fatigue due to changes in the temperature and relative humidity[10–13]; pollution of the membrane by contaminant ions.[14] The electrodes degradation mechanisms are mainly due to platinum dissolution and diffusion

Correspondence to: L. Flandin (lionel.flandin@univ-savoie.fr).

Contract grant sponsors: French National Agency for Research (ANR), PAN-H Program.

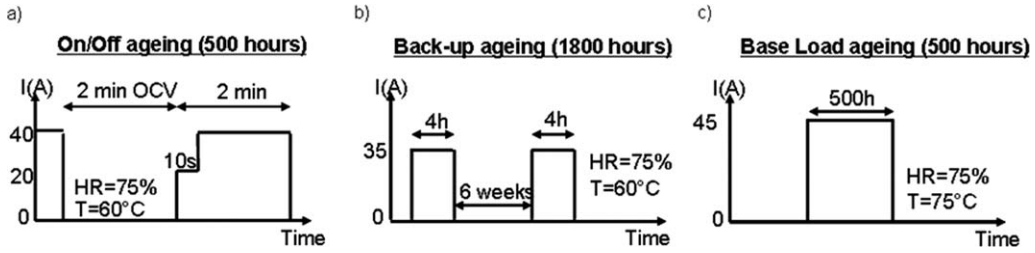

Figure 1 Description of current cycle undergone by twelve cells stack fuel cells: (a) on/off mode (500 h); (b) Back-up mode (1800 h); (c) Base load mode (500 h).

into the membrane,[15,16] to carbon surface oxidation,[17,18] due to chemical degradation of the electrode ionomer.[19] The degradation mechanisms of the GDL are mainly the resulting from the loss in hydrophobic character and change in the porous structure.[20,21] Degradation mechanisms in PEMFC operation studies are mainly performed with laboratory 1 to 12 cells self-made stack. Some parameters were identified as favoring the degradation of the MEA such as high cell voltage, change in humidity content,[22,23] On-off solicitation,[24] fuel and air starvation,[25] or also GDL characteristics.[26–29] However, few studies have been published so far on degradation mechanisms due to FC real applications.[30] Furthermore, the long-time ageing tests are often characterized with electrochemical techniques such as EIS,[31–34] which is not very sensitive to reveal microstructural changes within the polymeric phase of the MEA. The decrease in performance of fuel cells remain however ascribed to the degradation of the MEA, and to understand the degradation mechanisms and optimize the fuel cells operation, it seemed extremely important to define pertinent ageing markers within the MEA that closely relate to the use properties. The present work will focus on this goal with the help of *ex situ* characterization techniques at different scales (microstructural, interfacial, mechanical) on a large amount of MEA aged in laboratory and on-site with different power solicitation.

MATERIALS AND METHODS

Materials and fuel cells ageing tests

The samples under investigation were prepared through catalyst coating backing (CCB) and presented an active surface area close to 90 cm^2. The MEA were analyzed in the 5 layers (GDL/cathode/membrane/anode/GDL) form to prevent any changes related to layer exfoliation. The membrane used in this study is a commercial perfluorosulfonic acid (PFSA) which exact nature may not be disclosed. The binding agent added to the active layer was similar in nature. Prior to each measurement, the samples were stored at a constant temperature of 25°C and 60% RH. All the MEA were conditioned for at least 10 h in FC to eliminate possible residual components from the manufacturing before any characterization. The conditioned specimens were so assumed to be "un-aged." To avoid any operating effect, a cutting model was designed according to the gas path. For each technique, the samples were always taken at the same position within the MEA.

Accelerated laboratory ageing tests

Active ageing

The first durability experience consisted in operating a 12 cells stack fuel cell (FC) under different current solicitations. The profile of each test is described in Figure 1.

The on/off ageing test (a) was performed during 500 h (around 6500 cycles) with a cycle of 2 min at OCV, followed by 10 s at 21A and finally 1 min 50 at 40A. The operating conditions were established as a temperature of 60°C and an air relative humidity of 75% with a cathodic stoechiometry of three to avoid the flooding at high intensity, hydrogen was operated dry in dead end mode with intermittent purges, air/hydrogen pressures were 1.25/1 bar. The back-up ageing test (b) was run during approximately 1800 h. The cells were solicited at 35A during 4 h at 60°C and 75% RH with a stoechiometry of 2.5. The stack was then stored during 6 weeks in a climatic chamber at constant temperature and relative humidity before a later current solicitation. The base-load ageing test (c) was performed at 45A at 75°C and 75% RH with a stoechiometry of 2.5 for 500 h.

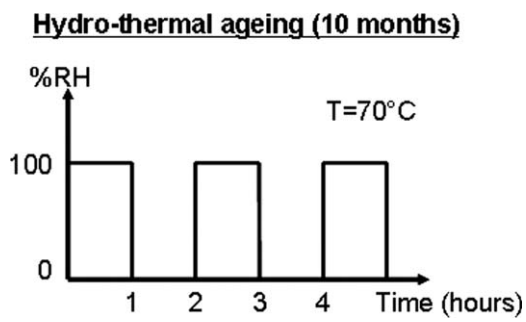

Figure 2 RH cycle scheme for the passive hydrothermal ageing.

TABLE I
Summary of the Main Properties of the On-Site Systems

Type of solicitation	Average power (kW)	Peak power (kW)	Ageing time (h)
Base-load	2–2.5	4–5	1500
Semi Base load	2	4	1500

Passive ageing

To study the influence of humidity changes on the MEA properties without any electrocatalytic activity, a hydro-thermal ageing test was set-up. The experiments conditions are described on Figure 2.

To achieve this ageing, the MEA were disposed in a climatic chamber at 70°C with a change of the relative humidity from 0 up to 100% every hour. The MEA were not stressed by any pressure during this ageing period. This test was performed for various periods of time, up to 10 months.

Real applications "on-site" ageing

The second durability experiment has consisted in operating a 2 × 55 cells stack "on-site" during around 1500 h under constant load linked to the current need of a remote telecom relay. The installation was of two types. The first system is qualified as base-load, i.e., main electrical alimentation of the relay whereas the second one called semi base-load is related to the fuel cell coupled with photovoltaic panels. Each system takes alternatively the power need of the relay. The semi base-load could be considered as on/off solicitation profile. The main properties of each system are described in Table I.

Ex situ postageing MEA characterization

Dynamical mechanical thermal analysis

Dynamical mechanical thermal analysis (DMTA) tests were performed with a MK-II Polymer Laboratories apparatus. The dimensions of the samples were 2.5 × 1 × 0.35 cm^3. Prior the test, the samples were gently stretched (1 mm/min during 5–10 s) to break the GDL and measure the viscoelastic properties of the sole membrane. Then, once the sample was positioned into the clamps, the membrane was dried during 1 h under N_2, and then solicited at different frequencies (1, 3, and 10 Hz) at a heating rate of 1°C/min from room temperature up to 250°C. Figure 3 shows the typical response of the storage modulus E′ and the tan δ as a function of the temperature. From this curve, the temperature T_α was defined at the maximum of the tan δ peak. This temperature can not be compared with the T_g (measured in DSC) with this kind of complex heterogeneous materials.

Scanning electron microscopy

The small samples from MEA were cut perpendicular to the flow channels. The dimensions of the samples were around 0.5 × 0.5 × 0.35 cm^3 and were analyzed on the cross section. Samples were embedded in an epoxy resin at ambient temperature. The reaction of the resin (Epofix from Struers) was nonexothermic and did not present dimensional variations which would have been harmful for the MEA. Then, the MEA cross section was polished until reaching a mirror effect.

The scanning electron microscopy (SEM) images were realized with a Leica Stereoscan 440 microscope. The thickness of the different layers (membrane, anode, and cathode) was computed with the help of ImageJ, program developed by Wayne Rasband at the National Institute of Health. After adjusting the color threshold, the thickness value was averaged over more than 700 lines for each picture.

Thermogravimetric analysis with mass spectroscopy

The thermogravimetric analysis with mass spectroscopy (TGA-MS) measurements were carried out with a simultaneous thermal analyser Netzsch TG-209 F1 Iris and coupled with a quadruple mass spectrometer, Netzsch, QMS 403 Aëlos II apparatus. The sample weight was around 8–10 mg, measured accurately. The test was run under air at a heating rate of 10°C/min. The loss weight and the ion current of selected fragment were recorded as a function of the temperature.

Tensile test

The tensile tests were conducted with an ADAMEL DY30 material testing system with operating conditions of ambient temperature and a relative humidity in the 50–60% range. The samples were cut as normalized dumbbell edge referred as B2 in the NF

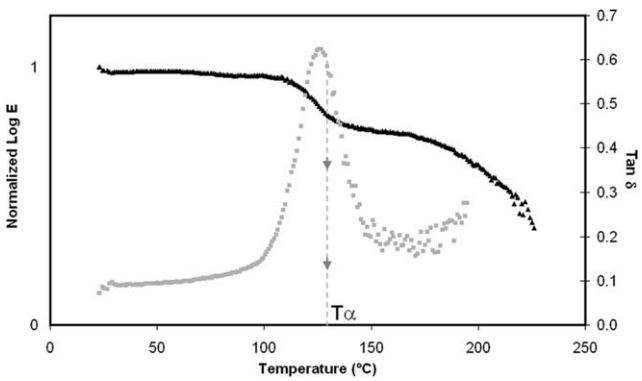

Figure 3 Illustration of the response of the normalized storage modulus and tan δ as a function of the temperature of a MEA.

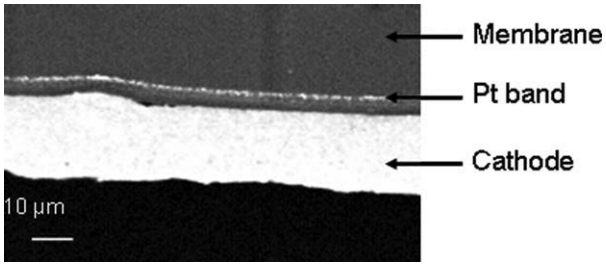

Figure 4 SEM image of the Pt migration at the cathode side observed with the base load and semi base load solicitations.

ISO 6239. The strain rate was of 5 mm/min. For each specimen, the thickness was taken as the average of five measurements distributed over the sample length. Figure 4 shows the typical raw response in force versus displacement for an un-aged membrane and an un-aged MEA. From the force versus displacement curves, two interesting parameters could be extracted. This first one is the decohesion energy (C) defined as the area between the MEA behavior and that of the un-aged membrane for a displacement ranging from 4 to 9 mm. The second probe is the total displacement at $1.25N$ ($D_{1.25}$).

MEA sampling for characterizations

One of the specificity of this work has consisted in the characterization of a large amount of MEA (around 80). The sample cutting profile was defined to strictly take up the samples at the same localization. Table II summarizes the number of MEA studied per ageing test and the number of samples per MEA.

The first approach of this work was to reveal some trends as a function of the type of ageing solicitations. Thereby, the box and whisker plot were used to display the results. This statistical approach consists of the median, the quartiles and the smallest and largest values in the distribution. Immediate visual of a box and whisker plot gives information to the center, the spread and the overall range of distribution.

RESULTS AND DISCUSSIONS

Macroscopic scale: Thickness evolution

Table III summarizes the membrane and electrodes thickness computed from SEM image for each solicitation, as well as the observation of Pt migration into the membrane (Fig. 4).[15,16] It is also important to notify the relatively important distribution of the results (2–3 µm). This accuracy determined with around 700 numerical data is ascribed to thickness distribution along the membrane.

Nonetheless, SEM analysis performed on the MEA which undergone different solicitations have revealed some trends. The 10 months hydro-thermal ageing and Back-up ageing tests did not show significant decrease in the layer thickness. It also results that On/Off solicitation does not appear as severe as reported in the literature.[7] In contrast, the membrane thickness is reduced after both base load solicitations as observed in the literature.[4,32] This decrease in membrane thickness is related to a chemical degradation of the membrane. In addition, the cathode thickness would tend to decrease after operating in on-site stacks. This degradation could be imparted to different mechanisms such as carbon support corrosion on fuel cells operation[17,18] or also due to binding agent degradation.[35,36] The decrease in either cathode or membrane thickness could also be related to the presence of Platinum into the membrane. Moreover, it seems that there is not necessarily a correlation between the diminution of the membrane and cathode thicknesses, but a correlation between the thinning of the membrane or cathode thickness with the migration of Pt into the membrane. The Pt^{2+} may thus also be responsible for membrane degradation trough a catalyst effect.

Macroscopic scale: Mechanical properties of MEA

The force displacement curve of the membrane (Fig. 5) shows typical elastic–plastic behavior composed by a first elastic region followed by a nonreversible plastic deformation after the yield stress point. Concerning the force-displacement response of the multilayer MEA (Fig. 5), distinctive parts related to three

TABLE II
Summary of the MEA Sampling: (a) Number of MEA Received Per Ageing Test; (b) Number of Samples Analysed Per MEA

(a) Number of MEA

Un-aged	Hydro-thermal	On/off	Back-up	Laboratory base-load	On-site base-load	On-site semi base-load
2	2 per month	12	12	12	14	14

(b) Number of samples per MEA

SEM	Tensile test	DMTA	TGA-MS
1–3	12	1-4	1–4

TABLE III
Summary of the Membrane and Electrodes Thicknesses Computed for Each Ageing Test

	Membrane thickness (μm)	Anode thickness (μm)	Cathode thickness (μm)	Platinum migration into the membrane
Un-aged	30.3 ± 1.9	13.7 ± 2.4	13.7 ± 2.2	No
Hydro-thermal (10 months)	26.3 ± 2.5	13.2 ± 2.9	13.7 ± 3.0	No
On/off	27.9 ± 2.3	14.0 ± 3.0	13.4 ± 2.9	No
Back-up	29.4 ± 2.1	15.2 ± 3.3	12.5 ± 2.9	No
Laboratory base-load	23.8 ± 2.0	13.4 ± 2.4	13.5 ± 2.4	Yes
On-site base-load	24.2 ± 2.3	12.2 ± 2.8	10.1 ± 2.0	Yes
Semi base-load	30.0 ± 2.2	12.6 ± 2.7	10.4 ± 2.0	Yes

different mechanisms can be distinguished. The first region (I) is due to the brittle behavior of the GDLs with the complete breakdown of the fibers at the maximum of the peak. Then, in the region (II) the presence of a plateau is observed. This plateau represents the decohesion at the membrane/electrodes interface induced by shear stresses. Once the decohesion is finished, the region (III) begins related to the membrane plastic deformation. Thus, the durability criteria extracted from this test to follow microstructural modifications of the MEA with ageing were the decohesion energy and the plastic displacement at 1.25*N*, as defined previously.

The hydro-thermal ageing has allowed to follow the mechanical properties changes of the MEA as a function of the ageing time. The force-displacement curves of the MEA over the 10 months ageing show interesting variations of behavior at different steps (Fig. 6).

First, the level of the plateau where the decohesion between the membrane and the electrodes occurred significantly decreased over time. The repeated solicitations at this interface due to the swelling of the membrane as a function of its humidity content (dry or wet), strongly affect the phase connectivity. The force required to shear this interface becomes lower with the ageing time. This result may originate from the diffusion of the oligomer into the membrane, or the molecular weight decrease within the membrane. This could also originate from the accumulated plastic strain at the membrane/electrode interface resulting in fatigue solicitation.

Second, an important change in the region III related to the membrane response was detected. The displacement recorded for a 1.25*N* force increased from 13 mm to 29 mm during the 10 months of hydro-thermal solicitation. This phenomenon is not yet well understood. Different unsupported mechanisms can be suggest such as the decrease of the molecular weight due to membrane degradation, or due to the loss of functional groups, or from a composite effect caused by the decohesion between the electrodes and the membrane promoting craks formation.

Figure 7(a) shows the evolution of the decohesion energy computed over the 10 months of hydro-thermal ageing time. The decohesion energy versus hydro-thermal ageing time significantly decreases up to negative values due to un-aged membrane reference. This drop in energy is significant after 6 months of hydrothermal ageing. Two zones were established (< 4 months on hydro-thermal ageing; and > 4 months) to rapidly estimate the degree of ageing of the MEA. These zones were drawn in Figure 7(b) and superimposed to results obtained from fuel cells operations.

Each ageing type, either laboratory or on-site, presents an average decohesion energy close to the

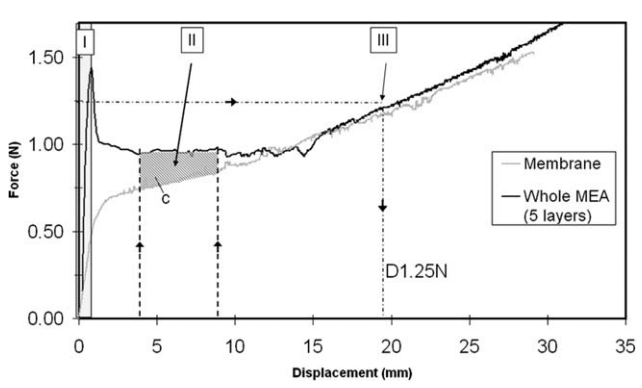

Figure 5 Engineering force-displacement curves on a membrane (gray) and a MEA (black) in tensile mode.

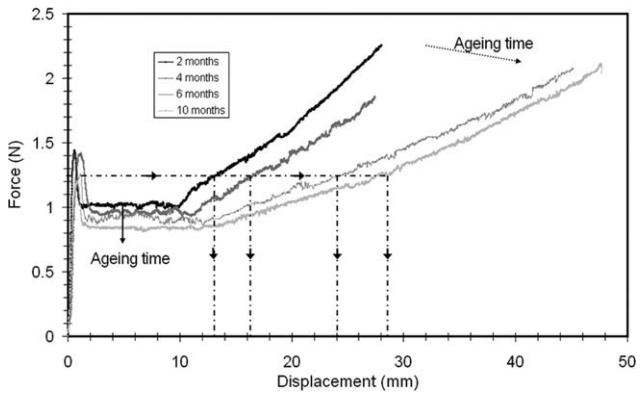

Figure 6 Force-displacement behavior of the MEA as a function of hydro-thermal ageing time.

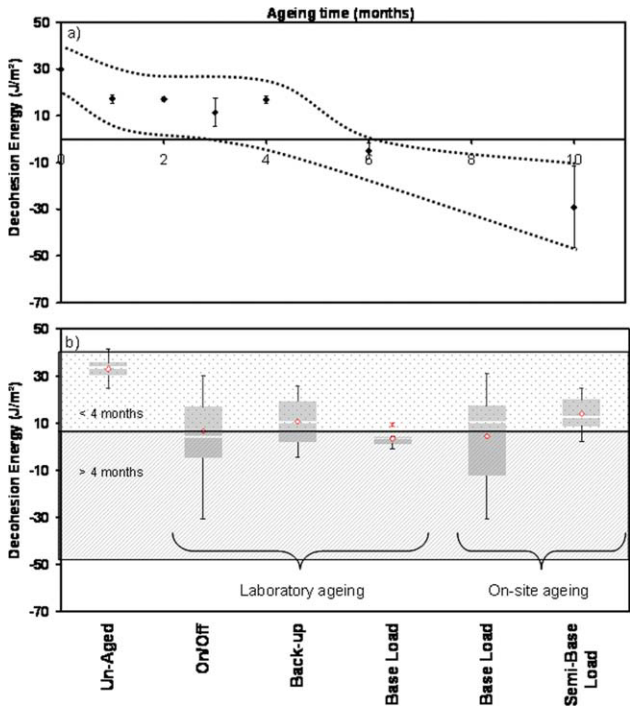

Figure 7 Evolution of the decohesion energy between membrane and electrodes. (a) evolution of this criteria as a function of the ageing time on hydro-thermal ageing; (b) Box whiskers representation as a function of the type of solicitation (laboratory and on-site). [Color figure can be viewed in the online issue, which is available at www.wileyonlinelibrary.com.]

accepted limit defined previously. This means that the FC cycling of start-up and shut-down during operation, so as constant load induce microstructural changes at the membrane/electrodes interface. Moreover, a large distribution of the results was observed not only inter-MEA but also intra-MEA. This could results from many parameters of the system such as position of the specimens in the MEA depending on the gas path, position of the MEA in the stack, clamping force anisotropy. These points will be detailed in a future work.

Similar data analysis for the displacement at 1.25*N* were done and reported in Figure 8.

The evolution of the displacement value at 1.25*N* also shows a significant change of behavior which occurs between 4 and 6 months of %RH cycling. In fact, the membrane increases its plasticity going from a displacement value around 20 mm up to 30–35 mm. As for cohesion energy, one behavior before 4 months hydrothermal ageing and one after 6 months were also distinguished. From this mechanical parameter, large differences between laboratory FC solicitations and on-site FC solicitations appear. Indeed, the 1.25*N* displacements for MEA coming from laboratories fuel cells are still in the tolerance area of < 4 months, whereas all the MEA measurements performed on MEA extracted from on-sites ageing stacks fall in the > 4 months area. It seems that a system power solicitation in real conditions and longer ageing time does increase the plasticity of the membrane. It is also difficult to quantitatively relate this plasticity to the decohesion energy. In fact, the semibase load solicitation MEA presents an acceptable decohesion energy even after 1500 h while the increase of the plasticity is one of the highest. This apparent contradiction reveals that craks or failure mode induced by the delamination between membrane and the electrodes are not the only causes for mechanical damage. Other parameters like changes in membrane microstructure would be of interest to correlate to better understand the ageing mechanisms of the MEA. This will be performed through DMTA and TGA-MS tests.

Molecular scale: Main relaxation temperature evolution

Table IV reports the main relaxation temperature T_α of the MEA for each ageing test (laboratory and on-site) performed during this work. A 5°C uncertainty was estimated using our experimental protocol; it mainly originates from mechanical coupling induced by the presence of both GDLs and electrodes.

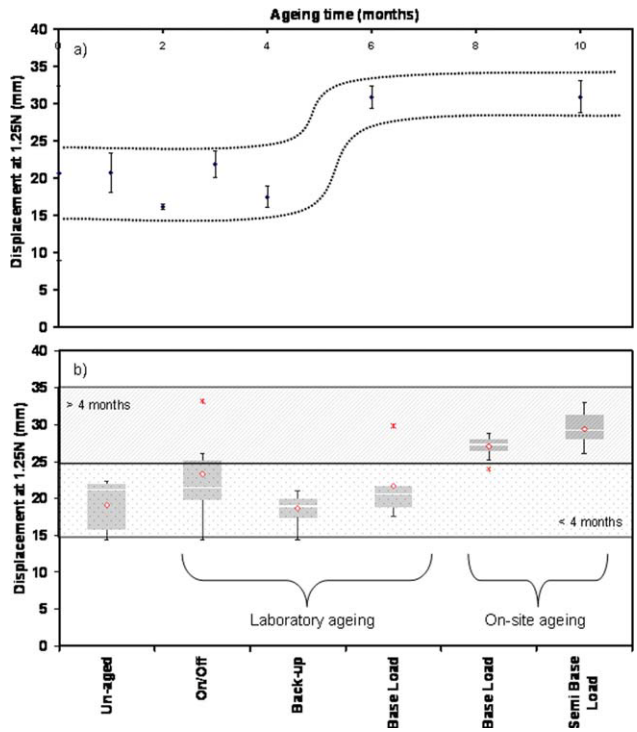

Figure 8 Evolution of the displacement at a strength value of 1.25*N*. (a) evolution of this criteria as a function of the hydro-thermal ageing time; (b) Box whiskers representation as a function of the type of solicitation (laboratory and on-site). [Color figure can be viewed in the online issue, which is available at www.wileyonlinelibrary.com.]

TABLE IV
Main Relaxation Temperature for Different Type of Ageing Solicitation

	T_α (°C)
Un-aged Membrane	125 ± 1
Un-aged MEA	125 ± 2
Hydro-thermal (4 months)	124 ± 2
Hydro-thermal (10 months)	128 ± 2
On/off	123 ± 5
Back-up	121 ± 4
Laboratory base-load	120 ± 5
On-site base-load	121 ± 3
Semi base-load	125 ± 1

The un-aged membrane and the un-aged MEA display a main relaxation temperature T_α around 125°C. The analysis of the aged samples of any ageing mode (passive, active, laboratory, or on-site) does not reveal any significant variation of this temperature. This indicates that no major changes occurred within the polymeric chains with the current ageing procedures. This later fact seems in agreement with chemical degradation proposed in the literature.[37]

Molecular scale: Thermal degradation of the MEA

Figure 9 shows a comparison of the TGA derivative weight signal between the individual components (membrane, and GDL/electrodes) and the MEA response.

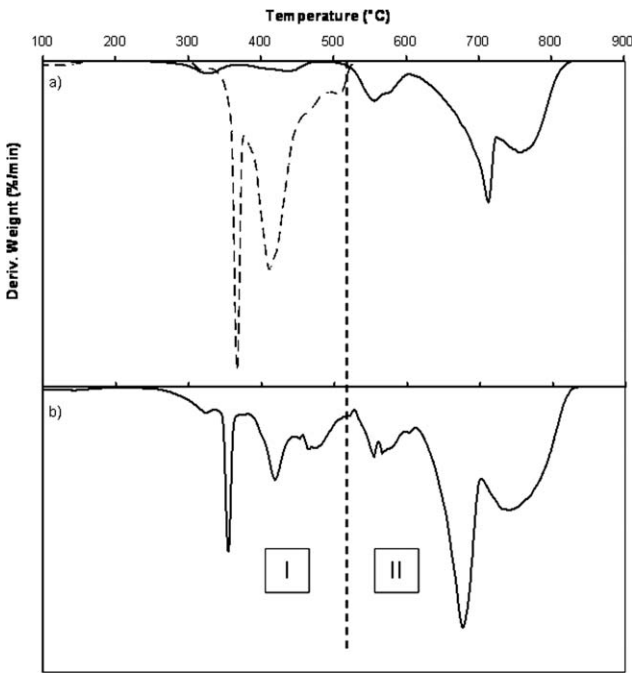

Figure 9 Comparison between the derivative weight signals: (a) individual components (membrane-dashed; GDL+AL-line); (b) whole MEA.

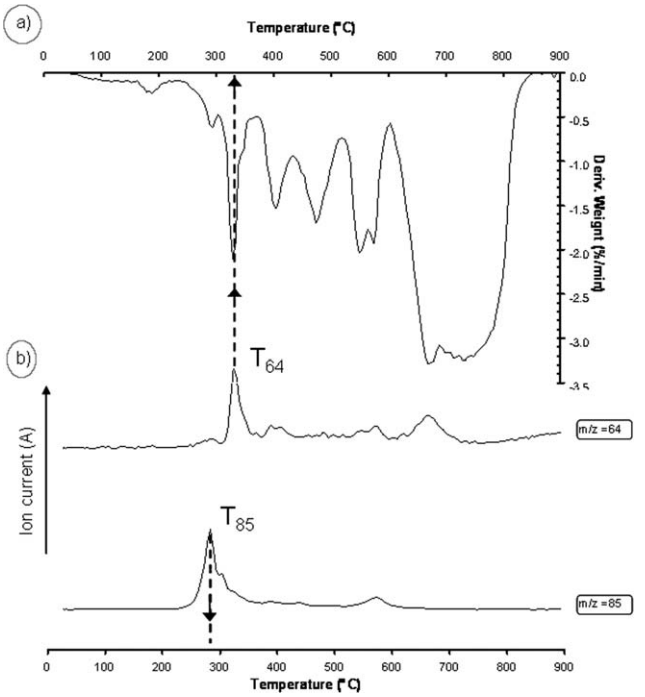

Figure 10 TGA-MS curves of an unaged MEA. (a) TGA derivative weight signal as a function of the temperature; (b) MS signals of fragment mass (64 and 85) as a function of the temperature.

Two regions are clearly identified within the MEA derivative weight signals. The region I mainly corresponds to the membrane response. However, the GDL/AL curves shows two peaks in this region (around 310°C and 450°C) which are due to some thermal degradation mechanisms of the active layer. The region II above 500°C is the thermal degradation response of GDL and carbon support.

Figure 10 shows a superposition of the derivative weight signal of an un-aged MEA and the MS signal of two fragments related to m/z 64 and m/z 85. The temperature at the *m/z* 64 curve maximum and the first maxima temperature of m/z 85 curves were extracted and defined as T_{64} and T_{85}, respectively.

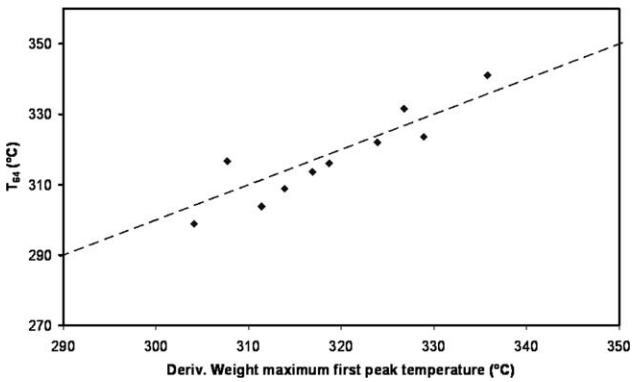

Figure 11 correlation between T-derivate and the T64.

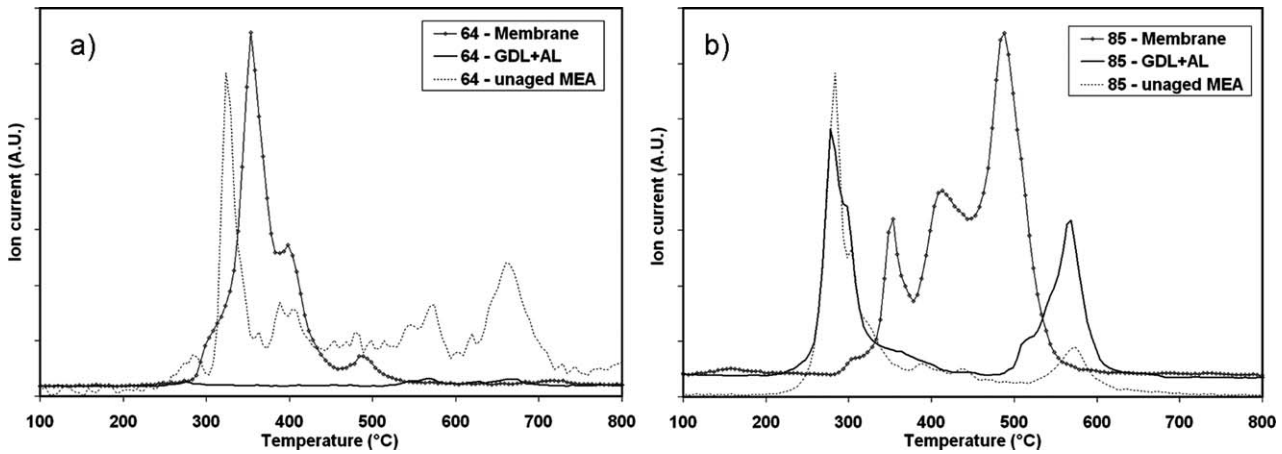

Figure 12 MS curves superposition of the individual components (membrane and GDL/AL) with an un-aged MEA for two fragments (64 and 85).

To study the thermal degradation mechanism modification of the membrane, the durability criteria of interest is the temperature at the highest peak of the m/z 64. The m/z 64 associated to the m/z 48 is related to the formation of the sulfur dioxide gas, SO_2 resulting from the thermal decomposition of functional sulfonic acid units.[38,39] Moreover, this temperature T_{64} is correlated to first peak maximum temperature of the TGA derivative curve (T_{derivate}) (Fig. 11). The analysis of the individual components by MS [Fig. 12(a)] clearly exhibits that the mass of 64 is strictly a fragment from the membrane. No evident signal was recorded for the GDL/AL around 300–400°C.

The second selected probe was the temperature at the maximum of the first peak for the m/z 85 fragment. Indeed, at temperature lower than 320°C, this fragment is mainly due to the GDL/AL response, Figure 12(b). This means that one of the thermal degradation mechanisms of the MEA which occurs at the lowest temperature corresponds to degradation or structural modification of the binding agent located in the active layers.

MS curves of the individual components (membrane and GDL/AL) and un-aged MEA were superposed to identify the localization of the fragments within the MEA (Fig. 12).

In the case of the hydro-thermal ageing test, numerous samples could be collected and data could be analyzed for each durability criteria and ageing time. Figure 13(a) shows the changes in thermal degradation of the mass fragment 64 over 10 months. T_{64} shows a significant variation after 4 months in hydro-thermal ageing test. During the first months of solicitation, the temperature decomposition computed was found between 310 and 330°C. After 4 months, the range increased rather suddenly from 310°C up to 355°C. Looking closer to the data, this change originates from the appearance of a bimodal distribution of the results for specimens aged 6 months and more. This behavior could be explained by an extremely localized measurement with a sample size around 4 to 5 mm^2. Nevertheless, to estimate the degradation of the MEA operating in stacks, two distinct zones related to TGA behavior below and above 4 months were drawn. Figure 13(b) shows box whisker of T_{64} for the different ageing modes in comparison with un-aged and hydrothermal ageing.

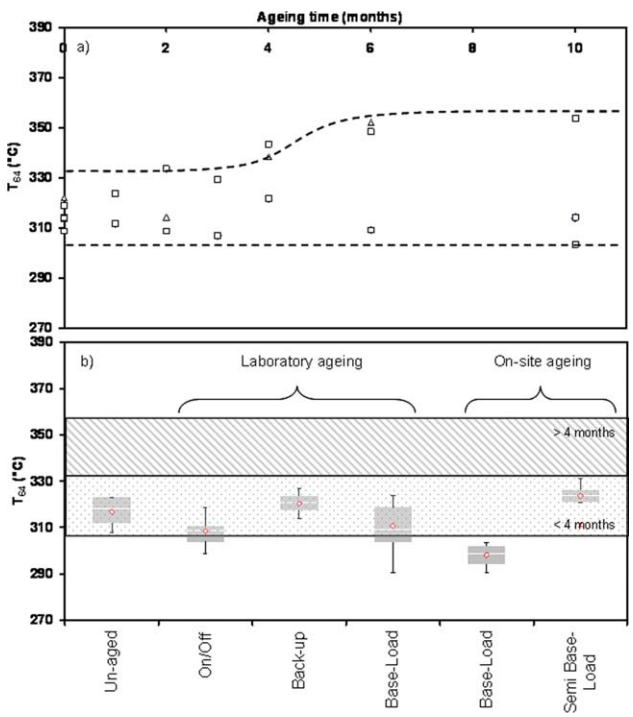

Figure 13 Evolution of the thermal degradation of the fragment mass m/z of 64. (a) evolution of this criteria as a function of the ageing time on hydro-thermal ageing; (b) Box whiskers representation as a function of the type of solicitation (laboratory and on-site). [Color figure can be viewed in the online issue, which is available at www.wileyonlinelibrary.com.]

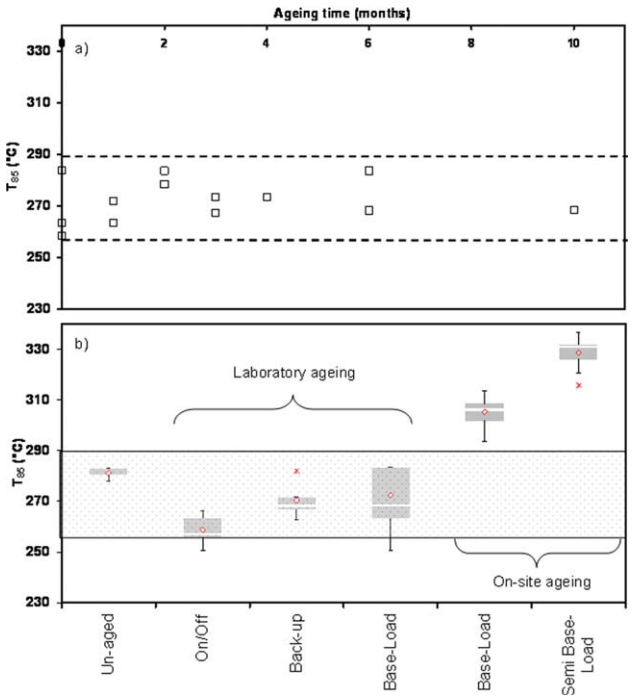

Figure 14 Evolution of the thermal degradation of the fragment mass m/z of 85. (a) Evolution of this criteria as a function of the ageing time on hydro-thermal ageing; (b) Box whiskers representation as a function of the type of solicitation (laboratory and on-site). [Color figure can be viewed in the online issue, which is available at www.wileyonlinelibrary.com.]

T_{64} displayed by MEA aged on different accelerated laboratory stacks were in the same range as the short time hydrothermal aged MEA. Thus, the thermal decomposition of the functional groups within the membrane was not affected by these solicitations. On the contrary, the analysis of the on-site base-load aged MEA has shown opposite trend than that of hydro-thermal ageing. Indeed, the T_{64} decomposition temperature decreases up to 290–300°C but still remain in the perfluorosulfonic acid membrane range of 275–400°C.[39]

Similar analysis was performed for T_{85}. The first step temperature T_{85} of the thermal degradation is not significantly modified by 10 months of dry-humid cycle [Fig. 14(a)]. The recorded temperatures range from 255 to 285°C. Identical temperature range is also found for MEA aged by all the laboratory tests [Fig. 14(b)]. However, significant change on T_{85} occurs for MEA aged on-site regardless of the current solicitation. Indeed, an increase of the temperature up to 310°C, i.e., close to the T_{64} was observed. In addition, no correlation with T_{64} could be done, and the chemical structure of this product could not be defined with certitude. This product was assumed to be related to the binding agent that cumulatively disappeared during the on-site FC solicitations.

CONCLUSIONS

MEA durability was investigated under laboratory accelerated tests such as fuel cell and passive hydro-thermal ageing processes with different load profile and under on-site power applications.

This first part of this work permitted to set-up different characterization techniques and procedures (SEM, DMA, TGA-MS, tensile test). Each test was adapted to the specificity of the five layers MEA samples without removing layers. The main results from these techniques were the definition of ageing markers. The most pertinent markers with the set of MEA and ageing procedure revealed to be (i) layer thickness, (ii) temperature at the maximum of the first peak of the m/z 85 in TGA/MS, (iii) plastic strain at 1.25N in tensile test, and (iv) the cohesion energy also measured in a tensile test.

These different criteria were first validated and calibrated as a function of the ageing time in the hydro-thermal electrochemically passive process. Most markers exhibited large changes between the fourth and fifth months of ageing. This means that in a passive mode the MEA microstructure at different scales (membrane/electrodes interface, membrane plasticity, membrane microstructure…) varied essentially simultaneously. The same markers were then employed for comparison with the fuel cell aged MEAs. It resulted that no systematic MEA degradation occurs after 500 h laboratory ageing regardless of the current profile. One exception is the presence of the Pt band within the membrane and the membrane thickness decrease for 500 h base-load tests. However, the 500 h laboratory on/off solicitation which is considered as one of the most severe type of ageing did not reveal advanced degradation state.

The 1500 h real use operating campaign with a base-load and a semi base-load linked with photovoltaic panels were compared with the MEA laboratory response. The MEA do not necessarily behave in the same way. As for 500 h base load laboratory, Pt band or membrane thickness decreases is detected in 1500 h operating MEA. On a mechanical point of view, plastic behavior of MEA is similar to those displayed by long time hydrothermal ageing. Nevertheless, based on TGA-MS experiments, both on-site ageing are more aggressive compared to the accelerated ageing tests. They induce significant changes on a chemical point of view in the active layers.

Considering these results, it appears more evident that more parameters from the macroscopic scale should be investigated to better understand the degradation mechanisms and their sources. The next step of this project will be to collect operating systems data to make correlation between the system and the MEA microstructural ageing mechanisms.

The authors thank all industrial and academic partners for MEA preparation, FC operation and numerous fruitful discussions.

References

1. Tang, H.; Peikang, S.; Jiang, S. P.; Wang, F.; Pan, M. J Power Sources 2007, 170, 85.
2. Merlo, L.; Ghielmi, A.; Cirillo, L.; Gebert, M.; Arcella, V. J Power Sources 2007, 171, 140.
3. Kinumoto, T.; Inaba, M.; Nakayama, Y.; Ogata, K.; Umebayashi, R.; Tasaka, A.; Iriyama, Y. J Power Sources 2006, 158, 1222.
4. Healy, J.; Hayden, C.; Xie, T.; Olson, K.; Waldo, R.; Brundage, M.; Gasteiger, H.; Abbott, J. Fuel Cells 2005, 5, 302.
5. de Bruijn, F. A. T.; Dam, V. A.; Janssen, G. J. M. Fuel Cells 2008, 8, 3.
6. Inaba, M.; Kinumoto, T.; Kiriake, M.; Umebayashi, R.; Tasaka, A.; Ogumi, Z. Electrochim Acta 2006, 51, 5746.
7. Lee, S.-Y.; Cho, E.; Lee, J.-H.; Kim, H.-J.; Lim, T.-H.; Oh, I.-H.; Won, J. J Electrochem Soc 2007, 154, B194.
8. Collier, A.; Wang, H.; Zi Yuan, X.; Zhang, J.; Wilkinson, D. P. Int J Hydrogen Energy 2006, 31, 1838.
9. Curtin, D.; Lousenberg, E.; Robert, D.; Henry, J. T.; Tangeman, P. C.; Tisack, M. E. J Power Sources 2004, 131, 41.
10. Escobedo, G.; K. R.; Nagarajan, G. S.; Schwiebert, K. E. ECS Trans 2006, 1, 303.
11. Tang, Y.; Karlsson, A. M.; Santare, M. H.; Gilbert, M.; Cleghorn, S.; Johnson, W. B. Mater Sci Eng A 2006, 425, 297.
12. Kusoglu, A.; karlsson, A. M.; Santare, M. H.; Cleghorn, S.; Johnson, W. B. J Power Sources 2007, 170, 345.
13. Solasi, R.; Zou, Y.; Huang, X.; Reifsnider, K.; Condit, D. J Power Sources 2007, 167, 366.
14. Cheng, X.; Shi, Z.; Glass, N.; Zhang, L.; Zhang, J.; Song, D.; Liu, Z.-S.; Wang, H.; Shen, J. J Power Sources 2007, 165, 739.
15. Xie, J.; Wood, D. L.; More, K. L.; Atanassov, P.; Borup, R. L. J Electrochem Soc 2005, 152, A1011.
16. Ferreira, P. J.; la O, G. J.; Shao-Horn, Y.; Morgan, D.; Makharia, R.; Kocha, S.; Gasteiger, H. A. J Electrochem Soc 2005, 152, A2256.
17. Knights, S. D.; Colbow, K. M.; St-Pierre, J.; Wilkinson, D. P. J Power Sources 2004, 127, 127.
18. Maass, S.; Finsterwalder, F.; Frank, G.; Hartmann, R.; Merten, C. J Power Sources 2008, 176, 444.
19. Kundu, S.; Foler, M. W.; Simon, L. C.; Abouatallah, R.; Beydokhti, N. J Power Sources 2008, 183, 619.
20. Gurau, V.; Bluemle, M. J.; De Castro, E. S.; Tsou, Y. M.; Mann, J. A.; Zawodzinski, T. A. J Power Sources 2006, 160, 1156.
21. Ihonen, J.; Mikkola, M.; Lindbergh, G. J Electrochem Soc 2004, 151, A1152.
22. Zhang, J.; Tang, Y.; Song, C.; Xia, Z.; Li, H.; Wang, H.; Zhang, J. Electrochem Acta 2008, 53, 5315.
23. Kim, S.; Hong, I. J Ind Chem Ind 2008, 14, 357.
24. Borup, R. L.; Davey, J. R.; Garzon, F. H.; Wood, D. L.; Inbody, M. A. J Power Sources 2006, 163, 76–81.
25. Taniguchi, A.; Akita, T.; Yasuda, K.; Miyazaki, Y. J Power Sources 2004, 130, 42.
26. Yan, W. M.; Hsueh, C. Y.; Soong, C. Y.; Chen, F. L.; Cheng, C. H.; Mei, S. C. Int J Hydrogen Energy 2007, 32, 4452.
27. Shimpalee, S.; Beuscher, U.; Van Zee, J. W. Electrochim Acta 2007, 52, 6748.
28. Lim, C.; Wang, C. Y. Electrochim Acta 2004, 49, 4149.
29. Park, G.-G.; Sohn, Y.-J.; Yang, T.-H.; Yoon, Y.-G.; Lee, W.-Y.; Kim, C.-S. J Power Sources 2004, 131, 182.
30. Du, B.; Guo, Q.; Pollard, R.; Rodriguez, D.; Smith, C.; Elter, J. J Miner Met Mater Soc 2006, 58, 45.
31. Mérida, W.; Harrington, D. A.; Canut, J. M. L.; Maclean, G. J Power Sources 2006, 161, 264.
32. Cleghorn, S. J. C.; Mayfield, D. K.; Moore, D. A.; Moore, J. C.; Rusch, G.; Sherman, T. W.; Sisofo, N. T.; Beuscher, U. J Power Sources 2006, 158, 446.
33. Liu, D.; Case, S. J Power Sources 2006, 162, 521.
34. Yan, X.; Hou, M.; Sun, L.; Liang, D.; Shen, Q.; Xu, H.; Ming, P.; Yi, B. Int J Hydrogen Energy 2007, 32, 4353.
35. Guilminot, E.; Corcella, A.; Chatenet, M.; Maillard, F.; Charlot, F.; Berthome, G.; Iojoiu, C.; Sanchez, J. Y.; Rossinot, E.; Claude, E. J Electrochem Soc 2007, 154, B1106.
36. Sompalli, B.; Litteer, B. A.; Gu, W.; Gasteiger, H. A. J Electrochem Soc 2007, 154, B1349.
37. Kundu, S.; Simon, L. C.; Fowler, M.; Grot, S. Polymer 2005, 46, 11707.
38. Wilkie, C. A.; Thomsen, J. R.; Mittleman, M. L. J Appl Polym Sci 1991, 42, 901.
39. Samms, S. R.; Wasmus, S.; Savinell, R. F. J Electrochem Soc 1996, 143, 1498.